NOVA
SCIENCE PUBLISHERS, INC.

FLY ASH COMPOSITES WITH POLYANILINE: SYNTHESIS, CHARACTERIZATION AND CONDUCTIVITY MEASUREMENTS

Himanshu Narayan

Hailemichael Alemu

Vernon S. Somerset

Emmanuel I. Iwuoha

Monica L. Hernández

July A. Hernández

Angela M. Montaño

José A. Henao

In: "Fly Ash: Reuse, Environmental Problems and Issues"

Editor: Peter H. Telone

ISBN: 978-1-60741-632-6 2010

400 Oser Avenue, Suite 1600
Hauppauge, N. Y. 11788-3619
Phone (631) 231-7269
Fax (631) 231-8175
E-mail: Main@novapublishers.com
http://www.novapublishers.com

In: Fly Ash: Reuse, Environ. Problems… ISBN: 978-1-60741-632-6
Editor: Peter H. Telone

Chapter 5

FLY ASH COMPOSITES WITH POLYANILINE: SYNTHESIS, CHARACTERIZATION AND CONDUCTIVITY MEASUREMENTS

Himanshu Narayan*[1], Hailemichael Alemu[2], Vernon S. Somerset[3], Emmanuel I. Iwuoha[3], Monica L. Hernández[4], July A. Hernández[4], Angela M. Montaño[4] and José A. Henao[4]

[1]Department of Physics and Electronics, National University of Lesotho, Roma 180, Kingdom of Lesotho, Southern Africa
[2]Department of Chemistry and Chemical Technology, National University of Lesotho, Roma 180, Kingdom of Lesotho, Southern Africa
[3]Department of Chemistry, University of the Western Cape, Private Bag X17, Bellville 7535, South Africa
[4]Grupo de Investigacion en Quimica Estructural, Universidad Industrial de Santander, Carrera 27 Calle 9, Ciudad Universitaria, Bucaramanga, Colombia

ABSTRACT

In the past few decades, Fly Ash (FA) has rapidly emerged as one of the most cost-effective and environment friendly resources rather than just being a waste material. A number of novel applications have been identified and are being exploited as well. The pozzolanic properties of FA make it a suitable candidate for cement replacement, as well as for the production of ceramics and glasses to be used as construction material. It can be utilized in the construction of embankments and structural fill; waste stabilization and solidification; mine reclamation; road sub-base; aggregate and mineral filler in asphalt concrete; soil amendment of soft soil and to increase bioavailability of nutrients in the soils, as well as adsorbent for heavy toxic metals. Other applications include production of roofing tiles, paints, metal casting, and as filler in wood and plastic products. Alkali rich FA can be used to neutralize the waste water from Acid Mine Drainage (AMD).

* Corresponding author: e-mail: h.narayan@nul.ls, Phone: +266 5221 3521, Fax: +266 2234 0000

Most of the current applications of FA, however, are primarily based on its microstructure and chemical composition only. Other physical and chemical properties of FA, and of the materials based on it, could possibly be utilized in other practical applications also. With this idea, we report in this chapter about the synthesis and characterization of a composite made of FA together with a very common conducting polymer: Polyaniline (PANI). The polyaniline/fly ash (PANI/FA) composites with various concentrations (20, 40 and 50 %wt) of fly ash were synthesized by the process of *in-situ* polymerization, by aging the starting materials (aniline and FA) before oxidative polymerization, and also by including poly-(styrene sulphonic acid) (PSSA). It was found that the process of aging assisted the composites to self-organize as nanotubes (cross-sectional diameters of 50-110 nm), and that involving PSSA, produced nanorods and nanofibres (diameters of 100-500 nm, length up to 10 μm). Powder X-ray diffraction (XRD), scanning electron microscopy (SEM), UV-vis spectroscopy, Fourier transform infrared (FTIR) spectroscopy, thermogravimetric analysis (TGA) and differential scanning calorimetry (DSC) were used to characterize the samples. Further, electrochemical analysis was performed and the dc-conductivity of the samples was measured as a function of temperature in the range 80-290 K. An expected decrease of conductivity was observed with addition of FA into PANI. The temperature dependence of the dc-conductivity for pure PANI and FA/PANI composites has been explained on the basis of the quasi one-dimensional variable range hopping (quasi-1D VRH) model. Excellent agreement was found between the experimental data and the theory.

INTRODUCTION

Originally treated as a waste material, fly ash (FA) is produced from the burning of coal, primarily in the coal-fired power plants. Several hundred million tons of FA is globally produced each year [1], and its disposal is still believed to be a worldwide problem. However, with the increasing number of applications, recognized and realized in the past few decades, FA does not seem to be a waste material any longer, but on the contrary, it is gradually proving to be one of the most cost-effective and environment friendly resources. Currently, only about a quarter of the total FA produced accounts for the part used in construction industry [1], and even if all the existing applications are included, the fraction being meaningfully utilized does not add up to more than 50% of the FA annually produced. In the recent years some serious efforts have been made worldwide in order to identify novel applications of FA, and some of the results are quite promising. Further development in this direction strongly depends on a better understanding of the various chemical and physical properties of the material.

In this chapter, we start with brief reviews on compositions of the FAs received from various origins, and some of their existing, and possible future applications. Then we present some results of our ongoing investigations on FA based composite materials. These composites were synthesized using two different FAs, one originating from South Africa, and the other from Colombia, with a conducting polymer polyaniline (PANI). Together with the results of the characterization (XRD, SEM, UV-vis, FTIR, TGA and DSC), we also present a discussion on the electrochemical behavior and the electrical conductivity of these composites.

Composition and Classification

Chemical composition is one of the most decisive factors for the suitability of FA for a certain application. A large variation is often observed in the compositions of FA from different sources, since it depends on the type of the coal burned. However, for the FAs originating from one region, the compositions of major constituents are usually found within a specific range. Compositions of typical FA samples from various countries are listed in Table 1 [2-6]. It is interesting to note that among the compositions listed here, the South African FA has highest percentage of alumina (37.20%), Indian FA has highest percentage of silica (58.12%), and Turkish FA has highest percentage of lime (47%).

Two major constituents of FA, which could often account for more than 60% of the material, are silica (SiO_2) and alumina (Al_2O_3). These two constituents, together with iron-oxide (Fe_2O_3), lime (CaO), magnesium oxide (MgO), and sodium oxide (Na_2O) are apparently present in all FAs. Other phases, such as, potassium oxide (K_2O), phosphorus pentaoxide (P_2O_5), titanium oxide (TiO_2), and sulfates, could also be present in some or other FAs, along with the traces of many other oxides and unburned carbon [2-7].

According to American Society for Testing and Materials (ASTM) C618 standards guidelines, FA can be classified into following two major classes based on its chemical composition that results from the type of coal burned [8]. The FA of Class F, which is produced from the burning of older anthracite and bituminous coal, contains less than 10% lime (CaO), and possesses pozzolanic properties. It requires a cementing agent, such as Portland cement, quicklime, or hydrated lime, which in the presence of water can react with the glassy silica and alumina present in the FA to produce cementitious compounds. On the other hand, the burning of younger lignite or subbituminous coal produces the FA of Class C, which generally contains more than 20% lime (CaO). As compared to Class F, this class of FA has higher alkali and sulfate contents. Besides the pozzolanic properties, Class C FA also has some self-cementing properties, and in the presence of water, it hardens and gains strength over time even without a cementing agent. Clearly, from the compositions of FAs listed in Table 1, only three, namely the ones from Greece, Spain and Turkey, fall under Class C. All others FAs in that list are of Class F.

Applications of Fly Ash

Applications of FA can be broadly classified into the following categories:

1. *Production of new materials*: A number of materials can be produced from the raw FA. Currently, the single largest utilization of FA is as a partial substitute for the raw materials in cement production. This is an extremely cost-effective use of FA, where its pozzolanic properties can be exploited. It provides not only an environment friendly option, but it is also known to improve the performance of the resultant concrete products. Replacement of cement with FA implies saving of the energy required, as well as reducing the carbon dioxide emission, associated with the cement manufacturing process. Bricks, mortars, blocks, shingles, paints and a number of other building materials based on FA are already in use [2,7,9].

Table 1.

Phase %	SiO_2	Al_2O_3	Fe_2O_3	CaO	MgO	Na_2O	K_2O	SO_3	P_2O_5	TiO_2
S. Africa [a]	41.50	37.20	2.45	9.95	2.27	0.53	0.83	0.50	1.35	2.65
Australia [b]	50.78	31.28	4.87	0.73	2.58	0.17	0.49		0.07	2.47
China [b]	43.52	20.53	10.47	8.26	2.52	1.19	1.25			0.91
Colombia [a]	53.90	28.00	6.53	4.73	1.47	0.66	1.77	0.40	0.76	1.92
Greece [c]	26.00	10.60	6.59	42.10	1.48	0.17	0.80	5.57		
India [d]	58.12	29.20	6.40	1.69	0.86	0.14	1.23	traces		
Indonesia [b]	34.21	15.19	5.91	13.52	5.61	6.88	1.14			0.71
Japan [c]	57.50	26.10	4.00	5.10	1.30	1.50	1.35	0.40		
Netherlands [c]	50.46	25.74	6.53	4.32	2.24	2.04	4.43			
Philippines [b]	46.16	31.91	8.67	6.85	1.52	1.47	0.85			1.62
Poland [c]	50.80	23.90	8.60	3.60	2.80	0.80	2.90	0.80		
Saudi Arabia [c]	52.30	25.20	4.60	10.00	2.20	0.60				
Spain [a,c]	49.80	17.30	8.70	24.90	1.90	0.30	1.70	4.30		
Taiwan [c]	48.75	23.21	4.15	3.93	1.00	0.24	1.10			
Thailand [b]	51.17	25.15	8.57	5.82	1.89	0.36	2.73			0.69
Turkey [c]	27.40	12.80	5.50	47.00	2.50	0.20	0.20	6.20		
UK [c]	50.09	28.10	11.70	1.62	1.54	0.28	0.62			
USA [a,c]	52.24	19.01	15.71	4.48	0.89	0.82	2.05	1.34		
Yugoslavia [c]	52.56	26.33	6.81	5.96	2.21	0.24	1.14	1.02		

[a] From Ref. [2,3]; [b] From Ref. [4]; [c] From Ref. [5]; [d] From Ref. [6]

Silica and alumina can be commercially recovered from raw FA following some specific processes [2,10]. Production of zeolites, such as faujasite, sodalite and zeolite A, is another important application of FA, because of the aluminosilicate glasses, which constitute major components of the latter [2,3,11-20]. The zeolites thus produced can be used in the purification of contaminated water [14]. Faujasite is used in the petrochemical industry as a catalyst, and anhydrous zeolite A in laundry detergents market.

Synthesis of high density, low porosity ceramic materials [5], mullite, glass-like materials and plastic composite materials from FA [2,10], have also been suggested. There are further possibilities of synthesizing aluminosilicate materials of commercial importance, such as kaolin, porcelain, etc., from FA, although not much work has been done in this direction.

2. *Environmental applications*: Water purification and waste management using FA constitutes another important category of applications. Chemical properties of FA can be exploited to deal with a number of environmental problems, e.g., in the process of wastewater treatment. In South Africa alone, a sizeable amount of wastewater is generated in the form of acid mine drainage (AMD) from the coal-mines. The FA can be co-disposed with AMD in such a way that the pH of the mixture has a known, pre-determined value, to serve a dual purpose. First, the two wastes are neutralized and much cleaner water is produced. Second, the collected solid residues could be used for production of high capacity ion exchange materials (e.g. zeolite, faujasite, etc.). These ion exchange materials can then be utilized for the

attenuation of metal species present in the neutralized FA/AMD processed waters [2,11,15-22].

FA can also be used as an adsorbant, as a replacement of active carbon, in the treatment of wastewater for the removal of a variety of organic compounds, such as polychlorinated biphenyls (PCBs), colours [23], and heavy metals, such as Ni, Cd, Pb, etc. [2,10].

3. *Soil amendments*: The alkaline properties of FA can be used in agriculture for amendment of acid-rich soils, which may not be appropriate for certain crops. Besides soil-neutralization, FA can also be a source of important crop nutrients, such as potassium and phosphorus [24]. However, the success of FA assisted soil amendments depends on a number of other factors too, e.g., chemical composition, texture, type of crops, etc. For example, the use of FA has been found to improve the yields of peanuts [9], but it was not recommended for cotton [25]. Studies have shown that addition of fine-textured fly ash to coarse-textured sandy soils can lead to a substantial increase in soil water-holding capacity, but also reduces soil hydraulic conductivity [26]. Sometimes, specific treatments of FA can be done in order to increase its effectiveness. For example, vermicomposting has been reported as a procedure for increased bioavailability of phosphorus in FA [27].

4. *Other applications*: Apart from the applications discussed above, raw FA can also be used in the construction of road subbase and pavements, structure fill (filler in wood and plastic products) and cover material [2]. As a unique engineering material, FA provides a better option as against the ordinary soil for the construction of embankments. Apart from these, the FA can also be utilized in the production of cellular concrete, geopolymers, roofing tiles, metal castings, etc.

It is however quite evident from the above discussion, that most of the current applications of FA are based mainly on its chemical composition and microstructure. The exploitation of other physical and chemical properties, such as, dc-conductivity and electrochemical behaviour, which seems to be rather limited until now, could possibly lead to several other, novel future applications. It is therefore crucial to explore various properties not only of the FA with various compositions, but also of the materials based on it.

For a number of meaningful applications, electrical conductivity is potentially one of the most important properties of a material. Usually, raw FA is rich in aluminosilicate materials (mullite, quartz, and alumina) and has a high electrical resistivity of the order of 10^{11}-10^{12} Ω.cm or even higher [28]. In comparison, porcelain, which is made from aluminosilicate materials (clay, quartz, alumina and feldspar) too, and is used in the high-tension ceramic insulators, has an electrical resistivity of the order of 10^{13} Ω.cm [29]. This implies that FA can possibly be used as a raw material in high-tension insulators applications, although not much work has been done along this direction. On the other hand, based on the requirements, the electrical properties of FA can be significantly modified, for example, by blending it into composites of suitable material, such as a conducting polymer.

Composites Based on Fly Ash

Recently, composites and blends based on conducting polymers (CPs) have emerged as a new class of potentially useful materials. A great deal of work is being done by many groups all over the world, and several classes of novel composites materials, like, organic/CP [30], CP/CP [31], CP/insulator [32], and more recently, inorganic/organic nanocomposites [33,34] have been synthesized and studied in detail. Although still in their elementary stage, these investigations have revealed the immense possibilities of technological exploitation of these materials.

Polyaniline (PANI) is one of the most interesting CPs, which is a suitable choice for various applications, such as, in solar cells, sensors, electromagnetic shields and rechargeable batteries' electrodes. Additionally, it is also known for its easy preparation methods and environmental stability [30,31,34-37]. Because of these unique properties, it has attracted special attention among all the CPs in the recent years. Electrical conductivity of PANI has been significantly modified by suitable doping. For example, doping PANI with malonic acid increases its conductivity by an order of magnitude [30]. Similarly, nanocomposites made of PANI and montmorillonite show a variation in room-temperature conductivity as much as eight to nine orders of magnitude depending on the PANI content [33].

Because of the above mentioned reasons, PANI was selected in this work as the host material for doping with FA in order to synthesize PANI/FA composites [38,39]. Interestingly, the room-temperature electrical conductivity of these composites was found to increase by more than ten orders of magnitude as compared to that of the insulating, raw FA [38]. In addition to this, the PANI/FA nanocomposites synthesized by aging the starting materials (aniline and FA) before oxidative polymerization, led to the formation of polymer nanotubes with cross-sectional diameters of 50-110 nm, and when the synthesis procedure involved poly-(styrene sulphonic acid) or PSSA, nanorods and nanofibres composites with diameters of 100-500 nm and length up to 10 μm were produced [39]. In this chapter, we report about the method of synthesis, characterization, electrochemical properties and electrical conductivity behaviour of these materials with various compositions.

EXPERIMENTAL

Synthesis of the Composites

The fresh FA used in these investigations was collected from local sources: Matla Power Station in South Africa and Termozipa Power Station in Colombia. The PANI/FA composites were synthesized according to the literature by the method of *in-situ* polymerization [32]. Aniline (AR) was purified by distillation before use and ammonium persulphate [APS, $(NH_4)_2S_2O_8$] and HCl were used as received. A 0.1 mol of aniline was dissolved in 1000 ml of 2 M HCl to form polyaniline (PANI). Varied amount (in weight %) of FA powder (e.g., 20 %wt, 40 %wt, 50 %wt, etc.) was added to the PANI solution with vigorous stirring. A 0.1 mol aqueous solution of APS, which acts as the oxidant, was added slowly with continuous stirring, to the aniline solution until the reaction mixture turned green. The reaction mixture was agitated continuously for another 8 h keeping the solution in an ice bath. The precipitate

formed was collected by filtration and washed with distilled water and acetone until the filtrate became colourless and free from aniline and SO_4^{2-}. The filtrate was dried at room temperature. The prepared PANI/FA composites contained 20%, 40%, and 50% by weight of FA in PANI. Same procedure was followed to synthesize composites with varying ratios of the primary constituents using both available types of the FAs.

Aged-PANI/FA composites were prepared using the South African FA only. For the synthesis of these composites, 0.1 M aniline solution containing 40 %wt FA was kept in the furnace at 100 ^oC for 48 h. The mixture was then cooled in an ice bath (0-5 ^oC) with vigorous stirring. After 30 min, 8 ml of 0.1 M aqueous solution of APS was slowly added with constant stirring of the reaction mixture. The stirring of the mixture continued for another 5 h and then it was placed in the ice bath for the next 5 h. After this, the vessel was removed from the bath and left at room temperature for 12 h. Then the product was collected by filtration, washed and dried, as described before.

The method reported by Cho *et. al.* [40] was adopted for the synthesis of composites that included PSSA also. 10.93 ml of PSSA was dissolved in 555 ml of water, to which 9.3 ml of 2 M HCl and 10.68 ml of aniline were added and placed in an ice bath with continuous stirring. 13.84 g of APS was dissolved in 80 ml of water and was slowly added to the reaction mixture in the ice bath and stirred for 12 h. The product (PANI/PSSA) was collected, washed and dried as previously described. For the preparation of PANI/PSSA/FA composites, the aniline solution also contained 40 %wt of South African FA before the APS was added.

Measurements

X-ray powder diffraction (XRD) measurements were done with a Shimadzu Lab XRD 6000 diffractometer (Shimadzu, Japan) using Cu-Kα radiation (λ = 1.5406 Å). Scanning electron microscopy (SEM) was carried out on a JSM 5600 electron microscope (Jeol Ltd., Japan) and a Hitachi X-650 Scanning Electron Microanalyser (Hitachi, Japan). Micrographs were obtained for the samples coated with a thin layer of gold and mounted on aluminium stubs using conductive glue. All the UV-vis absorbance experiments were performed at room temperature with UV/VIS 920 Spectrometer (GBC Scientific Instruments, Australia) using quartz cuvettes. The solution for UV-vis spectrometry was prepared by dissolving 0.005 g of the sample in 10 ml dimethylformamide. The Fourier Transform Infra-Red (FTIR) spectra of the samples were obtained with a Nicolet MAGNA-IR 760 Spectrometer in the range 4000-400 cm^{-1}. For FTIR, the pellets of samples were prepared using KBr. Thermal analyses (thermogravimetric analysis, TGA; and, differential scanning calorimetry, DSC) were carried out with SDT 2960 Simultaneous DSC-TGA (TA Instruments), in static air (with no air flow); and with DSC Q10-V8.1 Build 261 (Universal V-3.9A TA Instruments), in nitrogen atmosphere. Approximately 12 and 3.4 mg of each sample was analyzed in air and in nitrogen atmosphere, respectively, between 30 and 750 ^oC at flow rate of 10 ^oC min^{-1} using alumina crucibles.

Electrochemical measurements were performed with a BAS 50W potentiostat {Bioanalytical Systems (BAS), Lafayette, IN, USA}. A 20 ml conventional three-electrode cell system (BAS) was used that consisted of BAS Pt disk (1.77×10^{-2} cm^2) working and Ag/AgCl reference (3 M NaCl salt-bridge type) electrode, and a platinum wire auxiliary

electrode. Prior to use, the Pt electrode was cleaned by successive polishing with aqueous slurries of 1, 0.3 and 0.05 μm alumina powder (Buehler, Dorset, UK) followed by thorough rinsing with deionised water and acetone. The deionised water was prepared by passing distilled water through Milli-Q^{TM} water purification system (Millipore). The electrode was then placed in a cell containing 0.2 M sulphuric acid solution and the electrode potential was cycled at scan rate of 50 mVs^{-1} between an initial (E_i) to a switch (E_λ) potential of –1200 to +1500 mV, respectively. Cyclic voltammetry (CV) experiments were performed in a cell system consisting of the working, reference and counter electrodes placed in a paste of PANI composite prepared with 1 M HCl. Typically the electrochemical paste cell system consisted of homogeneous slurries made with 0.05 g polymer composite and 5 ml 1 M HCl. The paste cell was deaerated for fifteen minutes with argon, and a headspace argon atmosphere was maintained at very low flow rate during analysis. Voltammograms were recorded at 20 ^oC, scanning anodically (E_i = –200 mV, and E_λ = +1200 mV) at potential scan rates of 100-1000 mVs^{-1}.

For the electrical conductivity measurements, the powder samples were pressed into small pellets of 1 cm diameter with thickness about 1 mm. Pressure of about 10 tons was applied with a cold-press. The pellets so formed were brittle and therefore they were left for a week at room temperature (room-temperature annealing) so that they become hard enough for easy cutting. Then the pellets were carefully cut into parallelepiped shapes and mounted on a four-probe dipstick resistivity set up one by one. Electrical connections for current and voltage probes were made using silver paste and the stick was dipped into a liquid nitrogen dewar. The resistance of the samples was measured during the warming up of samples as the dipstick was pulled up gradually from the dewar, from about 80 K up to room temperature (290 K). After the measurements, the dc-conductivity $\sigma_{dc}(T)$ was calculated from the resistance data.

RESULTS AND DISCUSSION

X-ray Diffraction

Chemical composition of FA obtained from various sources has been analyzed and reported by many workers [2-7]. It is well known that the quartz (SiO_2), alumina (Al_2O_3) and mullite ($3Al_2O_3.2SiO_2$) are the three primary constituents of FA, which could account for more than 80% of the crystalline and glassy phases present in the material. Iron oxide (Fe_2O_3), calcium oxide (CaO), magnesium oxide (MgO) and titanium oxide (TiO_2) could be found as the secondary components in most of the FA samples, with some alkali oxides, sulphates and unburned carbon, likely to be found as traces.

Fig. 1 depicts typical XRD results obtained for the raw FA {fig. 1 (a)}, and for the PANI/FA composites with increasing concentrations (20%, 40% and 50% wt of FA) {fig. 1 (b)}. Presence of some crystalline phases with amorphous background is evident in all composites as well as in the raw FA. However, it is evident from the sharp peaks, that the Colombian FA has more crystalline parts, in comparison to the South African FA.

Crystalline SiO_2 can be identified as the primary constituent of FA from the two characteristic peaks at $2\theta = 20.9°$ and 26.6°, corresponding to the [100] and [101] reflection planes of quartz in both types of the raw FAs. The most intense peak of alumina at $2\theta = 25.6°$ ([012] plane), along with some smaller peaks at $2\theta = 22.6°$ [101], 35.2° [104], and at 43.4° [113] [11-3], shows the presence of crystalline Al_2O_3 in the South African FA. Presence of only the $2\theta = 35.2°$ [104], and probably of 59.8° [211] Al_2O_3 reflections in the Colombian FA implies the lower concentration of this phase present in the latter. Mullite ($3Al_2O_3.2SiO_2$) can be identified as the third primary constituent from a number of peaks, the most prominent ones at $2\theta = 22.8°$ [111], 35.5° [112] for the South African FA; and around 30.9° [121] [211], and $2\theta = 40.8°$ [131] for both of the FA samples. Moreover, some other metal oxides can be identified as the secondary constituents. For example, iron oxide (Fe_2O_3) peaks in both FA samples at $2\theta = 32.9°$ [110], and $2\theta = 54.3°$ [211][12-1]. Very small amount of calcium oxide (CaO) [peaks at $2\theta = 54.0°$ and 64.3°] is probably present as well in both of the FAs. However, small fraction of anatase titanium oxide (TiO_2) ($2\theta = 34.0°$ [110]) seems to be present only in the South African FA. Other constituents may also be present in the raw FA samples in negligible amounts. From the amorphous background observed in the XRD spectra, predominantly in the South African FA sample, it is evident that also the glassy phases of all these oxides constitute a significant part of the material. These results are very much in-line with the compositions of these FAs listed in Table 1.

Pure PANI shows a characteristic XRD peak at $2\theta = 25.9°$, that corresponds to the emeraldine salt (ES-I) phase of the polymer [41,42]. As reported earlier by Raghavendra *et al* [32], the PANI/FA composites show a sharp peak at $2\theta = 26.6°$, which is evident in our XRD results {fig. 1 (b)}. As the FA concentration increases, the height of $2\theta = 25.9°$ PANI peak gradually diminishes and a peak around $2\theta = 26.1°$, increases and becomes more prominent. This new peak is essentially a combination of the PANI peak ($2\theta = 25.9°$) and the peaks due to the constituents of FA around the same 2θ value. For example, as mentioned earlier, two main constituents of FA, namely, quartz and alumina peak at 26.6° and 25.6°, respectively [one more constituent, the anatase titanium oxide (TiO_2) also peaks at $2\theta = 25.8°$, although its concentration in FA is insignificant when compared to that of quartz and alumina]. Therefore, as the FA concentration increases, the PANI peak gradually disappears. In the XRD plots, this occurs as a gradual shift of peaks near $2\theta = 25.9°$ towards slightly higher 2θ values.

Scanning Electron Microscopy

A typical SEM image of pure FA at 4000x magnification is shown in fig. 2. Cenospheres of size ranging approximately from 1 to 5 μm are visible in the picture as spherical balls. Up to 20% of fly ash consists of cenospheres, which are lightweight spheres of silicate glass filled with nitrogen and carbon dioxide that float in water [43].

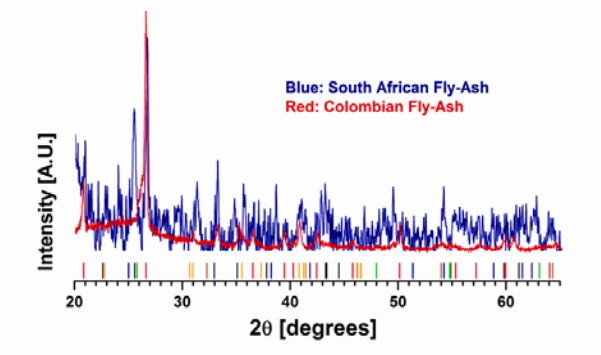

(a)

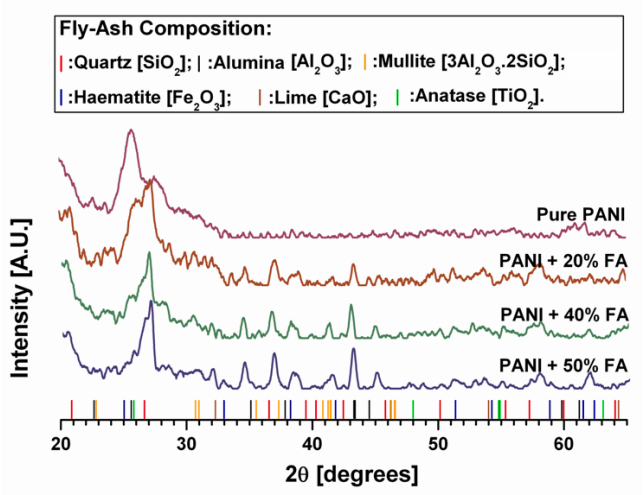

(b)

Figure 1: X-ray diffraction patterns for (a) Raw fly-ash; and (b) PANI/FA composites with different FA concentrations. Expected peak-positions of various constituents are shown by vertical bars.

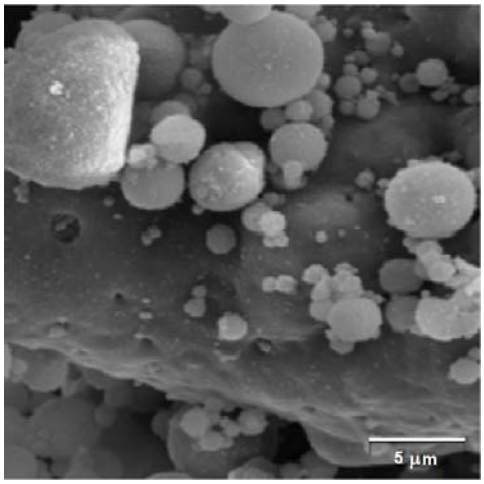

Figure 2. SEM picture of raw fly-ash.

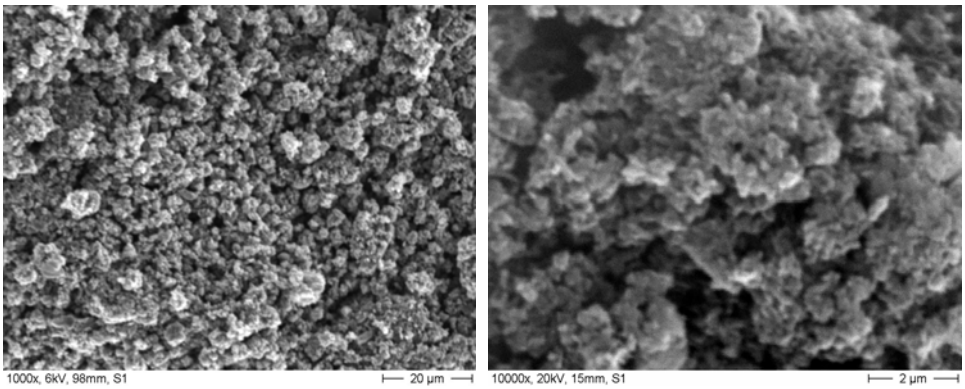

Figure 3. SEM pictures of pure PANI at two magnifications.

For pure PANI and the PANI/FA composites, SEM was recorded at two different magnifications, i.e., 1000x and 10000x. Fig. 3 shows typical SEM micrographs of pure PANI at the two magnifications. It is apparent from the picture that the material is homogeneous with the particle size ranging from 4 μm to 10 μm, with most of the particles around 5-6 μm size. It may also be noted from the SEM that the bigger particles are agglomerations of smaller, well-connected grains. The good connectivity among grains is expected to facilitate good electrical conductivity in this sample.

The SEM images of the PANI/FA composites with 20, 40 and 50 %wt of FA at the same two magnifications of 1000x and 10000x are shown in figs. 4 (a), (b) and (c), respectively. From the SEM pictures, it is evident that granularity increases with addition of FA in PANI, although the pure PANI appears to be more granular (at 10000x) than the composites. A careful observation of figs. 4 (b) and (c) reveals the presence of FA cenospheres in the composites. The cenospheres are more clearly visible as spherical balls of 1-2 μm size in the fig. 4 (b) at higher magnification.

Moreover, the grain size seems to decrease as the FA concentration increases. For example, in the composite with 20 %wt FA, the grains are much bigger than the scale in the SEM, i.e., 20 μm, whereas in the composite with 50 %wt FA, the size ranges from a few μm to about 10 μm. Again, the bigger particles seem to be agglomerates of smaller grains. This may also be looked upon as the decreasing grain-connectivity with increasing FA concentration in these composites. This feature is more evident in the SEM pictures at lower magnification. Expectedly, it should be reflected as a decrease in the electrical conductivity with increasing FA concentration.

The SEM picture of aged PANI/FA composite taken at 5000x magnification is shown in figure 5 (a). This composite was prepared by aging aniline with 40 %wt of FA before polymerization. Nanotube clusters of PANI/FA with average cross-sectional diameters of 50-110 nm are clearly visible in the micrograph. Synthesis of composites without the aging of aniline with FA, did not lead to nanostructures (e.g., fig. 4). This indicates that the metal oxides present in the FA activate the self organization of the polyaniline in tubular morphology [44-46]. The SEM micrograph of PANI/PSSA/FA is presented in fig. 5 (b). This was prepared with 40 %wt of FA. Inclusion of PSSA has apparently caused the aggregation of the polymer-precursors into nanorods that have an average length of 10 μm and cross-sectional diameters of 100-500 nm. Preparation of the PANI/PSSA/FA nanorods did not

require aging of the aniline and FA before addition of the APS. Additional investigations showed that aging of aniline/FA/PSSA mixture before polymerization did not alter the morphology of PANI/PSSA/FA. This implies that PSSA acts to stabilize the morphology of the composites. Similary, studies with PSSA and aniline alone (without FA) did not lead to any nanostructure morphology. From these observations, it may therefore be concluded that the metal oxides present in the FA play an important role in determining the nature of the final product. Also, the nanostructured morphology of the products can be stabilized either by aging, or by the inclusion of an appropriate additional component such as the PSSA.

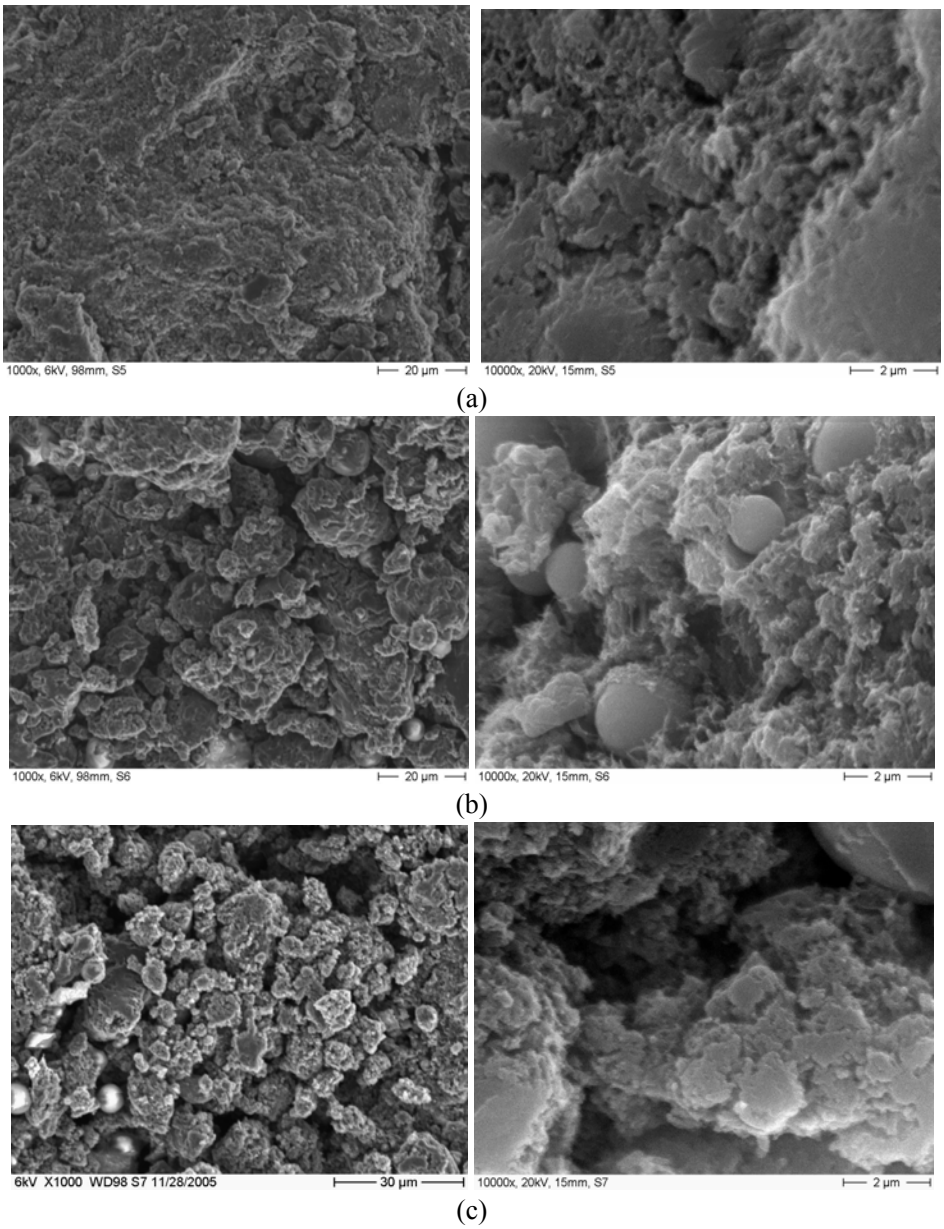

Figure 4. SEM pictures of PANI/FA composites at two magnifications. (a) PANI + 20 %wt FA, and (b) PANI + 40 %wt FA (c) PANI + 50 %wt FA.

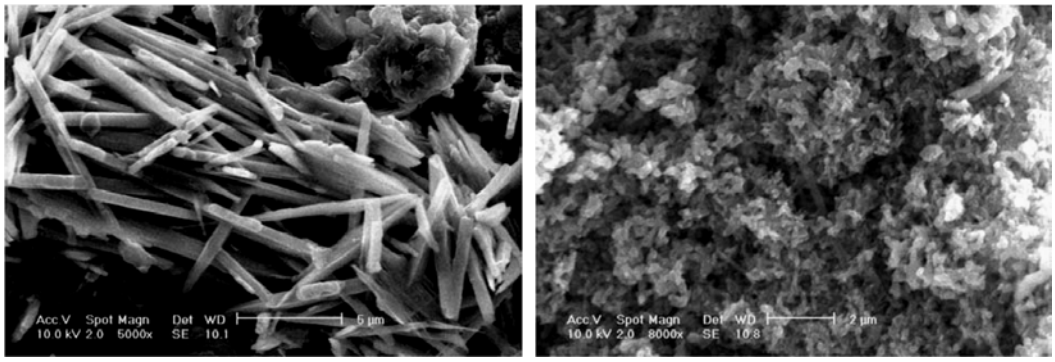

(a) (b)

Figure 5: Scanning electron micrographs of (a) Aged PANI + 40%wt FA (b) PANI/PSSA + 40%wt FA.

UV-vis Spectroscopy

Figure 6 shows the UV-vis spectra of the PANI/FA composites. In order to understand the UV-vis of PANI/PSSA/FA nanorods, the UV-vis of PANI and other PANI composites were also investigated. Fig. 6 (a) is the spectrum of aged PANI/FA nanotubes and fig. 6 (b) represents the UV-vis spectrum of PANI/PSSA/FA nanorods. The spectra of these two FA composites show two distinct peaks around 320 nm and 630 nm, which are characteristic of the PANI emeraldine base [40,44,47]. This indicates that nanostructured PANI composites are stabilized in the emeraldine base redox state. The peak at 320 nm is attributed to π–π^* transition of benzoid rings and the peak at 630 nm is attributed to the charge transfer excitons of the quinoid structure. Comparatively, PANI/PSSA and PANI/FA prepared without aging show clear similarity in their UV-vis spectra, particularly with the complete absence of the absorption maxima at 320 and 630 nm, which is associated with the stabilization of the composite in the emeraldine form. Rather the two composites show absorption peaks at 450 nm and around 800 nm. The 450 nm peak is due to polarons, and the peak at 680-800 nm is due to the doping level [40]. The peak at 450 nm gives an indication that the PANI is in the salt form (doped). This peak is also observed in pernigraniline salts. Polyaniline that does not contain either PSSA or FA shows four absorption peaks. There are peaks at 340 nm and 370 nm associated with π–π^* transition of benzoid rings and another peak at 600-650 nm (charge transfer excitons of the quinoid structure), which are characteristic of emeraldine base [48]. The peak at 450 nm shows the formation or presence of pernigraniline salt. Comparison of the PANI and PANI/PSSA/FA spectra shows that FA stabilizes the polyanilines in its emeraldine form.

Fourier Transform Infrared Spectroscopy

Figure 7 shows the FTIR spectra of PANI and 40 %wt FA in PANI. The characteristic peaks observed in the spectrum of PANI are due to the quinoid ring absorption at 1630 and 1150 cm^{-1}, absorption of benzoquinone at 885 cm^{-1}, the absorption due to benzenoid at 1375 and 1500 cm^{-1}, and the broad band for the N-H stretching at 3400-3100 cm^{-1} [32,49]. These

absorption bands are clear indications of the existence of the quinoid and benzenoid rings in the polymer chain. The bands at 1630 and 1150 cm^{-1} are characteristic of the emeraldine salt (ES-I) form of PANI (as also observed from the XRD). The presence of these peaks also indicates that the emeraldine salt is composed of quinoid and benzenoid moieties [49-52]. The intense and sharp band at 1630 cm^{-1} further indicates the relative abundance of the quinoid ring in the polymer structure. The IR spectrum of the FA/PANI composite in most of the cases resembles that of PANI indicating the existence of PANI in the emeraldine salt form. Slight shifts and additional peaks are observed in the range 2500-3000 cm^{-1}; 1300-1500 cm^{-1} and 1100-1300 cm^{-1}. The shifts and the additional characteristic peaks may be attributed to the presence of silica and other metal oxides present in FA. The IR spectrum of FA (spectrum not shown) gave a very broad peak in the range 1500-400 cm^{-1}. The broadening of the peak could be due to the merging of the IR peaks that arise from the absorption of the various metal oxides present in FA [32]. The IR spectra of 20 %wt FA in PANI and 50 %wt FA in PANI do not exhibit much variation in the characteristic peaks.

Thermal Analysis

The thermal behaviour of the raw FA and the different PANI/FA composites was investigated by Thermogravimetric Analysis (TGA) and Differential Scanning Calorimetry (DSC).

Thermogravimetric Analysis: The TGA (in air atmosphere) results are shown in figs. 8 (a) and (b). For the raw FA {fig. 8 (a)}, only about 0.5% of weight loss was observed up to 500 °C, which may be attributed primarily to the elimination of the moisture content of raw FA. Beyond 500 °C, a weight loss of about 5.2% has been recorded, which may be due to the complete burning off unburned carbon content [53]. Such a small weight-loss due to heating in air, from room-temperature up to 500 °C and even beyond, suggests a possible application of the FA as a fire-proof material. It is also noteworthy here that for such applications, the FA could be made more suitable by removing the unburned carbon content from the raw material.

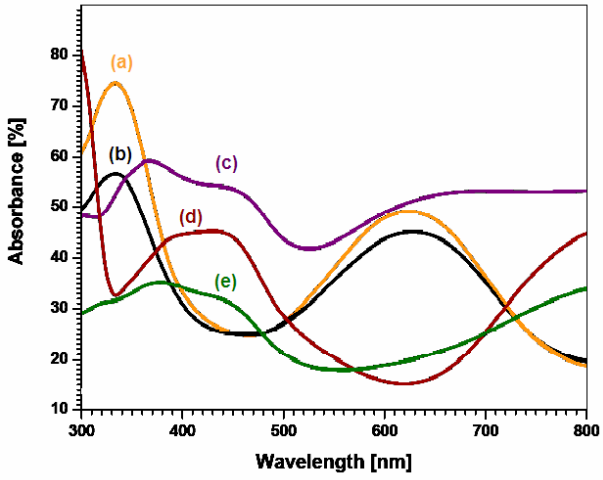

Figure 6: UV-vis spectra of polyaniline-fly ash composites with, (a) Aged PANI + 40 %wt FA, (b) PANI + PSSA + 40 %wt FA, (c) Pure PANI, (d) PANI + PSSA, (e) PANI + 40 %wt FA. Samples were prepared in dimethylformamide.

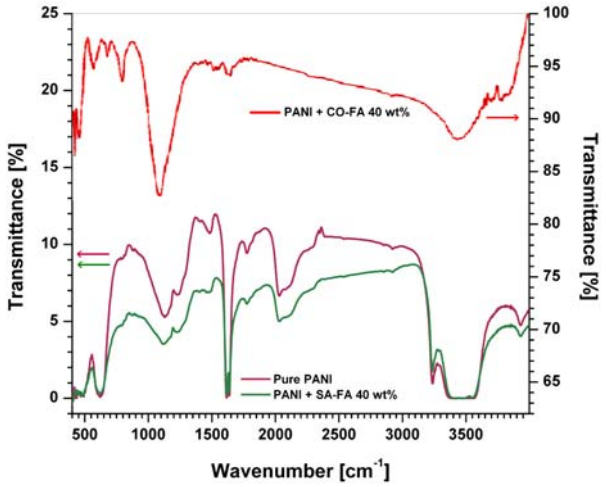

Figure 7. Infrared spectra of pure PANI and PANI + 40%wt FA.

The steady weight lose in air {fig. 8 (b)} observed for the PANI/FA composite samples, as well as for pure PANI, in the temperature range 80–450 ^{o}C is attributed to the elimination of adsorbed water (up to 30%) from both the oxide and polymer surface and acid dopant [54-56]. In this temperature range, there is no significant weight lose for the raw FA sample {fig. 7 (a)}. In addition to this, a well-differentiated behaviour marked by a strong weight loss in the temperature range 470–700 ^{o}C is observed for pure PANI and PANI/FA composites. This has been attributed to the degradation of the skeletal polyaniline chain structure [54-56]. Using the TG data, a plot of % weight lose versus % FA added in PANI gave a straight line with correlation coefficient of 0.990 indicating a good ratio of FA to PANI in the synthesized samples. Based on the TG data, the amount of polyaniline in each sample was assigned, corresponding to the following (in weight percent): 100.0; 83.9; 73.5; 69.6 for the samples: PANI; 20% FA in PANI; 40% FA in PANI and 50% FA in PANI, respectively. The above values are reasonably acceptable since a certain amount of the added FA in each sample would be expected not to form precipitate with PANI.

Differential Scanning Calorimetry: DSC measures the temperatures and heat flows associated with transitions in materials as a function of temperature or time in controlled atmosphere. DSC thermograms of PANI and PANI + 40%wt FA samples were recorded from room temperature up to about 600 ^{o}C. There are three endothermic peaks in the curves of fig. 9 of DSC for PANI and PANI + 40%wt FA, respectively. The first peaks have minima at 116.5 and 121.4 ^{o}C, respectively. These peaks are attributed to the removal of adsorbed water from both the oxide and polymer surface and fusion of PANI [59]. Minima of the second peak are at 244 and 298 ^{o}C, respectively, resulting from the complete removal of chemically active organic molecules. Fig. 9 (b) for PANI + 40%wt FA differs significantly from fig. 9 (a) as these endothermic peaks are minimized due to the higher content of FA particles confirming the structural changes after the incorporation of FA. The third peak appears at 296 and 438 ^{o}C, respectively. The shapes of these peaks are not well-defined and therefore could not be resolved.

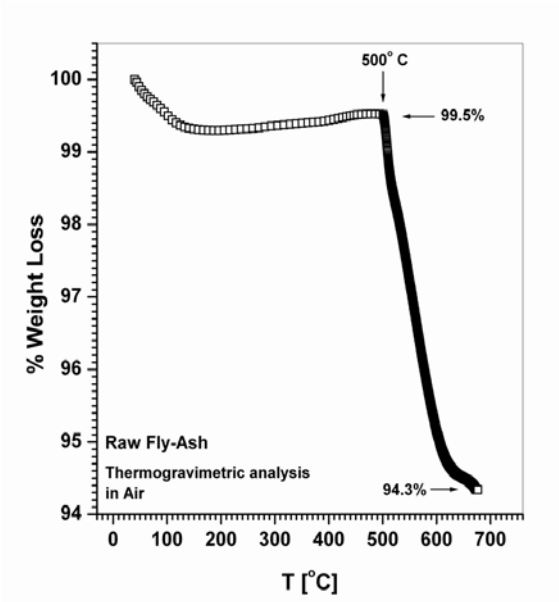

(a)

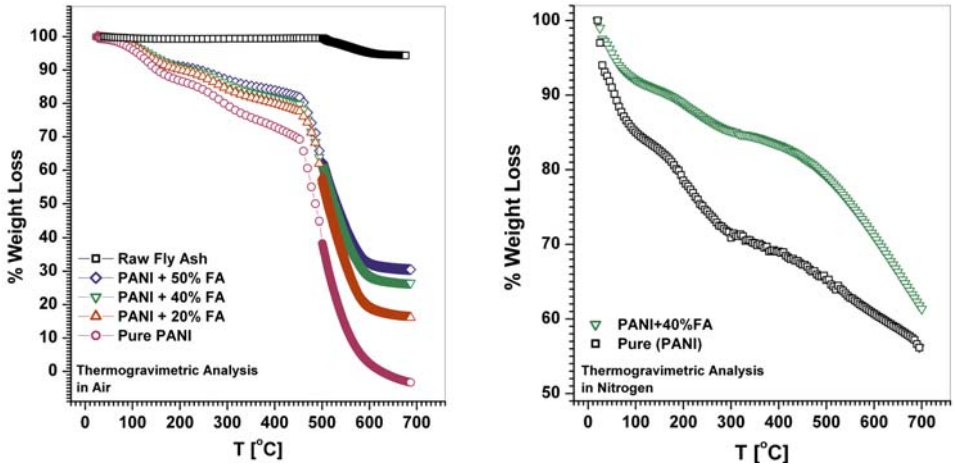

(b) (c)

Figure 8. Thermogravimetric curves obtained at 10 ^{o}C min^{-1} for (a) Raw FA in air atmosphere, (b) PANI/FA composites with different FA concentrations and pure PANI in air atmosphere, and (c) PANI + 40%wt FA composite and pure PANI in nitrogen atmosphere.

Electrochemical Properties

Cyclic voltammogram of PANI/PSSA/FA is shown in fig. 10. The redox peaks in the figure have been assigned using Pekmez formalism [60,61]: the first redox peak corresponds to the leucoemeraldine/leucoemeraldine radical cation (A/A´), the second to the emeraldine radical cation/emeraldine (B/B´) and the third to the pernigraniline radical cation/pernigraniline (C/C´). From the experimental design the voltammograms represent the electrochemical behaviour of the PANI composite at high potential scan rate. Only electrode

processes (electron transfer reaction at the electrode and any accompanying physical or chemical process) that have rate constants comparable to the fast potential scan rates (200-1000 mVs^{-1}) are discernible in the voltammograms. The 200 mVs^{-1} cyclic voltammogram (CV) of PANI/PSSA/FA have formal potentials, $E^{0'}_{(200\ mVs^{-1})}$, values of 105 mV (A/A′), 455 mV (B/B′) and 670 mV (C/C′). The corresponding cathodic to anodic peak current ratio, $I_{pc} / I_{pa\ (200\ mVs^{-1})}$, is 'unity' for all the three redox couples. However, at higher scan rates (500-1000 mVs^{-1}) the $E^{0'}$ value of the A/A′ redox couple vary with scan rate while those B/B′ and C/C′ are independent of scan rate within the limits of experimental error of ±10 mV. For example, the $E^{0'}_{(1000\ mVs^{-1})}$ values are 157 mV (A/A′), 465 mV (B/B′) and 660 mV (C/C′). The $I_{pc} / I_{pa\ (1000\ mVs^{-1})}$ values are 0.7 (A/A′), 1.0 (B/B′) and 0.8 (C/C′). These results indicate that the redox species exhibit quasi reversible electrochemistry at scan rates lower than 200 mVs^{-1}. But at higher scan rates the $I_{pc} / I_{pa\ (1000\ mVs^{-1})}$ values of 0.7 for the A/A′ redox couple means that the anodic process represented by A′ consist of electron transfer reaction at the electrode coupled to a diffusion process that is detectable only at fast scan rates, with the result that the anodic currents are higher than the cathodic currents and $E^{0'}$ values shift anodically with scan rate. The diffusion processes being detected at high scan rates could be intra-paste charge transfer within the electroactive polymer paste or intra-molecular charge transportation along the polymer backbone. The later event is more likely since $\Delta E^{0'} \{= E^{0'}_{(1000\ mVs^{-1})} - E^{0'}_{(200\ mVs^{-1})}\}$ value is only 50 mV which is less than 65 mV normally associated with surface-bound electroactive polymers undergoing charge propagation along the polymer chain.

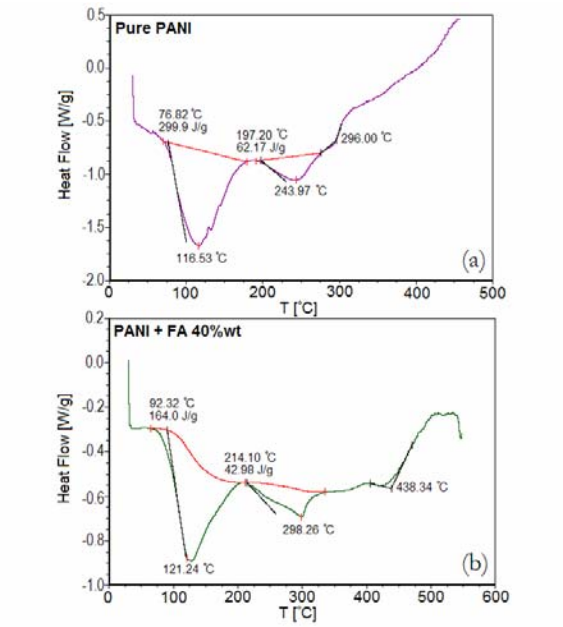

Figure 9. Differential scanning calorimetry results (a) for pure PANI and (b) for PANI + 40%wt FA composite.

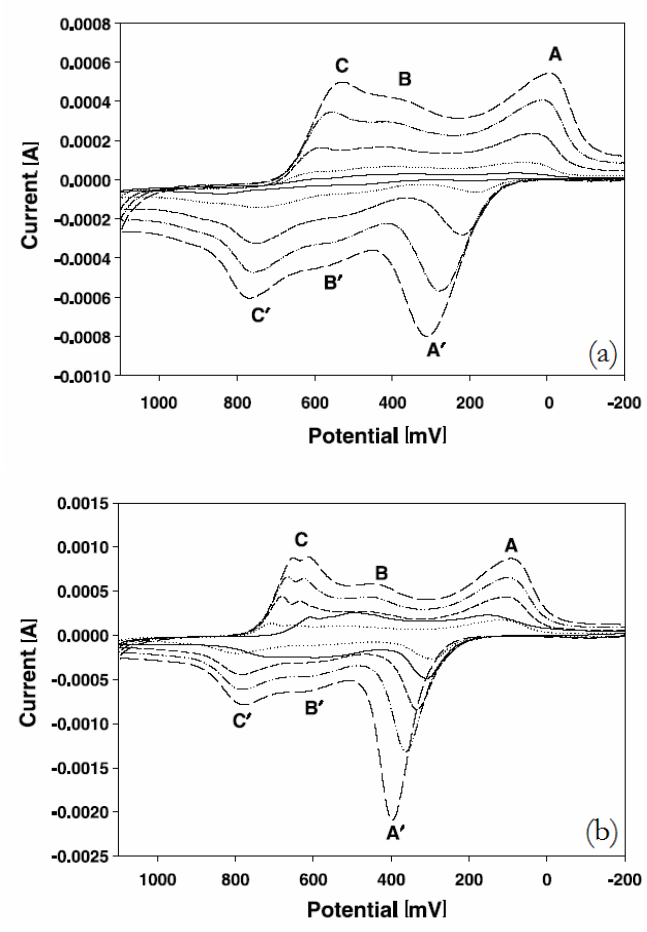

Figure 10. Multi-scan rate cyclic voltammograms for (a) PANI/PSSA/FA (40%) and (b) PANI/PSSA paste in 1 M HCl performed at of 100, 200, 500, 750 and 1000 mVs^{-1} (from inside outwards). (A/A´) leucoemeraldine/leucoemeraldine radical cation; (B/B´) emeraldine radical cation/emeraldine; (C/C´) pernigraniline radical cation/pernigraniline.

Figure 10(b) shows that the electrochemistry of PANI/PSSA is similar to those of PANI/PSSA/FA nanorods. The three redox couples of the 200 mVs^{-1} voltammogram display fairly reversible electrochemistry as shown by the $I_{pc} / I_{pa\,(200\ mVs^{-1})}$ value, which is approximately unity for each of the redox couples. But at 1000 mVs^{-1}, when the contribution of other fast processes become evident in the voltammograms, the $I_{pc} / I_{pa\,(1000\ mVs^{-1})}$ value drops to 0.4 for A/A´ and increases to 1.2 for C/C´. This shows that the charge propagation is more effective when the polymer is in the form of leucoemeraldine radical cation or pernigraniline radical cation, and for the emeraldine or its radical cation, charge transportation does not make significant contribution to the overall current. Changing from PANI/PSSA to PANI/PSSA/FA decreases both $E^{0'}_{(200\ mVs^{-1})}$ and $E^{0'}_{(1000\ mVs^{-1})}$ values. The effect of this is that FA causes a cathodic shift in the $E^{0'}$ values of the polymer irrespective of the redox state of the material.

Table 2.

Polymer	Redox peak	Conductance σ_{redox} [S]	$E^{0'}_{(200\ mVs^{-1})}$ [mV]		$E^{0'}_{(1000\ mVs^{-1})}$ [mV]	
PANI/PSSA	A´	2.63×10^{-2}	A/A´	205	A/A´	250
	B´	0.70×10^{-2}				
	C´	3.00×10^{-2}	B/B´	525	B/B´	530
	C	1.00×10^{-2}				
	B	0.90×10^{-2}	C/C´	750	C/C´	715
	A	2.00×10^{-2}				
PANI/PSSA/FA	A´	2.10×10^{-2}	A/A´	105	A/A´	160
	B´	0.53×10^{-2}				
	C´	2.40×10^{-2}	B/B´	455	B/B´	495
	C	0.70×10^{-2}				
	B	0.55×10^{-2}	C/C´	670	C/C´	660
	A	1.00×10^{-2}				

A: leucoemeraldine; A´: leucoemeraldine radical cation; B: emeraldine radical cation; B´: emeraldine; C: pernigraniline radical cation; C´: pernigraniline.

Conductance profile of all the six redox states of the PANI/PSSA/FA composites can be estimated from the multiple potential scan rate cyclic voltammetry data. This conductance of the redox states (denoted by σ_{redox}) is different from the normal conductance measured using a four point probe or conductivity cell. These latter two methods give the net overall dc-conductance (denoted by σ_{dc}) of the material, which is discussed in the next section.

The conductivity profile of the six individual redox states, σ_{redox} can be obtained by applying the classical Ohm's relation to the results of multiple potential scan rate cyclic voltammetry. In this method, the conductance of the redox states is given by,

$$\sigma_{redox} = \Delta I_v / \Delta E_v ,$$

where, $\Delta I_v = I_{p(1000\ mVs^{-1})} - I_{p(200\ mVs^{-1})}$, and $\Delta E_v = E_{p(1000\ mVs^{-1})} - E_{p(200\ mVs^{-1})}$.

The calculated values of the conductance for all the redox states of PANI/PSSA/FA and PANI/PSSA are collected in Table 2. Using this procedure, the average value of conductance for all the six redox states of the material is estimated to be 1.21×10^{-2} S for PANI/PSSA/FA and 1.7×10^{-2} S for PANI/PSSA. A general decrease in the conductance of the redox states of the composite is also observed as the morphology changed from the nanotubular PANI/PSSA to nanorodular PANI/PSSA/FA. These calculated values of σ_{redox} for the nanocomposites are in good agreement with the values reported for similar materials [62,63]. Another important observation is that the conductance increases as the nanorod composite is oxidized, A´ → B´ → C´ (Table 2). This trend is apparently related to the polarons associated with the formation of pernigraniline redox state. However, the emeraldine redox state (B´) exhibits low conductance values in both PANI/PSSA/FA (0.7×10^{-2} S) and

PANI/PSSA (0.53×10^{-2} S) as compared to the two other redox states, which may be due to the combined effect of occurrence of π–π^* transition of benzoid rings, and the formation of charge transfer excitons of the quinoid structure that is characteristic of emeraldine.

Electrical Conductivity

The results of dc-conductivity (σ_{dc}) measurements for pure PANI and two different compositions of PANI/FA composites are shown in fig. 11 in the temperature range 80-290 K. Shown in the inset of this figure is the experimental data. It may be noted that the resistivity (ρ_{dc}) of pure PANI as well as that of the composites decreases with increasing temperature showing their semiconducting nature. The value of temperature coefficient of resistivity (TCR) for pure PANI around room-temperature as calculated from our plots is -2.8×10^{-3} Ω.cm.K^{-1} at 0-10 ^{o}C range, which is comparable with a reported value of -4.0×10^{-3} Ω.cm.K^{-1} at 20-30 ^{o}C range [64]. However, considering the difference of temperature ranges, the value of TCR calculated from our graph is slightly lower than expected. Nevertheless, σ_{dc} for pure PANI was found to be 4.17 S.cm^{-1} (ρ_{dc} = 0.24 Ω.cm) around 285 K (12 ^{o}C), which is in very good agreement with the reported average value of 4.37 S.cm^{-1} at 20 ^{o}C [64].

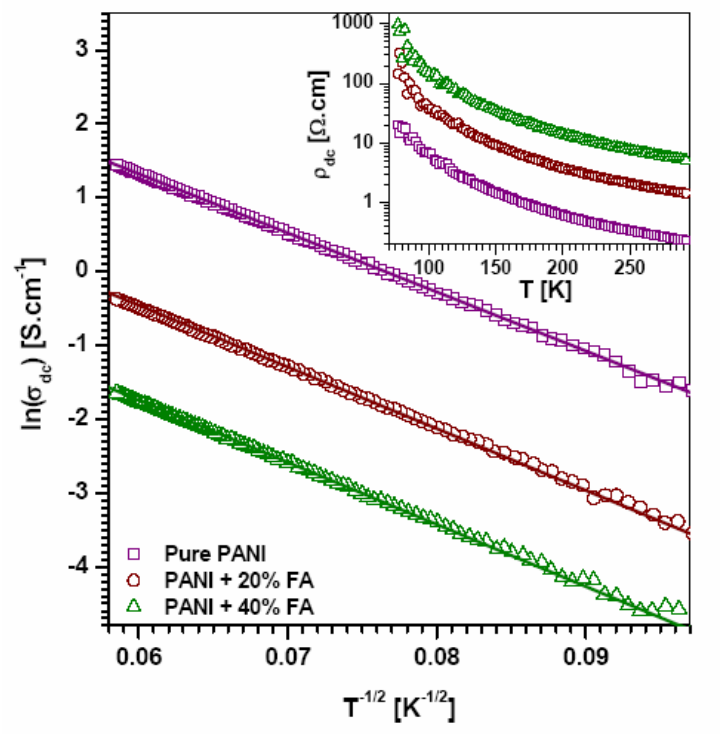

Figure 11. Temperature dependence of dc electrical conductivity (σ_{dc}). Best-fit according to the expression 1 (see text) are shown with solid lines. The inset shows the original experimental resistivity (ρ_{dc}) data as a function of temperature.

It may also be observed in fig. 11 that the conductivity $\sigma_{dc}(T)$ decreases with the increasing concentrations of FA. For the composites with 20 %wt and 40 %wt of FA in PANI, the values of σ_{dc} around room temperature (285 K) are 0.81 S.cm^{-1} (ρ_{dc} = 1.23 Ω.cm) and 0.21 S.cm^{-1} (ρ_{dc} = 4.76 Ω.cm), respectively. The TCR calculated from the plots for the composites are 8.6 x 10^{-3} Ω.cm.K^{-1} and 3.5 x 10^{-2} Ω.cm.K^{-1}, respectively, for the 20 %wt and 40%wt of FA in PANI. Evidently, as expected, the TCR as well as the room temperature conductivity decreases (resistivity increases) with the addition of FA in PANI.

In order to explain the temperature dependent conductivity behaviour of our samples, we assume that polymer chains are extended through the disordered regions and they connect the 'crystalline islands'. In this picture, charge carriers may diffuse along the electrically isolated disordered chains but are always capable to get localized because of the 1D nature of the chains. In such a situation, the temperature dependence of σ_{dc} for PANI and the composites may be explained on the basis of the quasi one-dimensional variable range hopping (quasi 1D VRH) model [33,65-67]. Within the framework of this model, σ_{dc} is given by the relationship,

$$\sigma_{dc} = \sigma_0 \exp\left[-\left(T_0/T\right)^{1/n}\right], \quad (1)$$

with the value of $n \approx 2$ for 1D hopping ($n \approx 3$ for 2D hopping, and $n \approx 4$ for 3D hopping). Here, the quantity σ_0 is also temperature dependent, but its dependence may be neglected when compared to the stronger dependence of the exponential term. T_0 is given by the relationship, $k_B T_0 = \dfrac{16}{L_{\|} N(E_F) z}$. In this expression, $L_{\|}$ is localization length, $N(E_F)$ is the density of states at Fermi level, z is the number of nearest-neighbour chains. Effectively, T_0 is the energy barrier for electrons to hop between localized states.

To fit our experimental σ_{dc} data for PANI (pure), we have used in equation 1, the reported value of T_0 = 6400 K [66]. As evident from the figure, a very good agreement was found between experimental data and the theoretical straight line. For the composites with 20 %wt and 40 %wt of FA in PANI, however, the best fit was achieved by using the value of T_0 equal to 6500 K and 6700 K, respectively. This increase in T_0 is expected with increase of FA percentage in PANI. Since T_0 is inversely proportional to the localization length $L_{\|}$, it means that as the FA percentage increases, $L_{\|}$ for the charge carriers in the composites decreases. As a result, the charge carriers become more localized, and thus are less free to move. Consequently, the conductivity decreases with increasing FA concentrations. In terms of T_0, this means that addition of FA in PANI increases the energy barrier required for hopping of electrons, and thus makes the conduction less easy. Therefore, it may be

concluded that the quasi one-dimensional hopping is the mechanism responsible for electrical conductivity in PANI/FA composites.

CONCLUSION

Rather than just being a waste material, fly-ash is rapidly emerging as a highly cost-effective and environment friendly resource. It is currently being used in the production of a number of new materials, water treatment, soil amendment, etc. However, most of the current applications are primarily based on the microstructure and chemical composition of the fly-ash. Other physical properties, such as, the electrical conductivity, could possibly lead to more novel applications. With this idea, we have presented in this chapter the results of our investigation on the synthesis, characterization and conductivity measurements of electrically conducting composites made of fly-ash (FA) and polyaniline (PANI). Fly-ash from two different sources, one South African and the other Colombian, were used and composites with various concentrations of fly ash (20%, 40% and 50%) were synthesized. The process of synthesis involved *in-situ* polymerization, aging of the starting materials (aniline and FA) before oxidative polymerization, and also the addition of poly-(styrene sulphonic acid) (PSSA). The resulting composite samples as well as the raw materials were characterized by XRD, SEM, UV-vis spectroscopy, FTIR spectroscopy, TGA and DSC.

Presence of some crystalline phases with amorphous background was evident in the XRD pattern of raw FA as well as in all the composites. However, apparently the Colombian FA had more crystalline phases, in comparison to the South African FA. The XRD pattern of pure PANI showed the presence of the emeraldine salt (ES-I) phase. As the concentration of FA increased in the composites, a small gradual shift of peaks around $2\theta = 25.9°$ towards higher 2θ values was also observed, which was attributed to the merging of the ES-I peak of PANI with those due to the FA constituents, which peak around the same value of 2θ. The SEM pictures of the raw FA, pure PANI and FA/PANI composites showed increasing granularity with addition of FA in PANI and the existence of the spherical FA particles (cenospheres). More interestingly, the SEM results also demonstrated the self-organization of PANI/FA nanocomposites as nanotubes (cross-sectional diameters of 50-110 nm) when aniline was aged with fly ash over a period of 48 h before oxidative polymerization. However, the requirement of aging aniline and FA before polymerization could be eliminated by the addition of PSSA in the reaction mixture. This process led to the self-organization of the polyaniline composites as nanorods (diameters of 100-500 nm, length up to 10 μm). Both the nanorod and nanotube FA composites of PANI showed similarity in their UV-vis absorption spectra at 320 nm indicating the stabilization of the nanostructured material in the emeraldine state. FTIR spectra of PANI and FA/PANI composites indicated the existence of the quinoid and benzenoid rings in the polymer chain of PANI. These spectra also supported the XRD result that the polymer used in this work was the emeraldine salt (ES-I) form of PANI. The thermogravimetry curves showed a clear and marked difference between PANI, FA, FA/PANI composites, where the major weight losses were associated with the degradation of the skeletal polyaniline chain structure. The TG analysis also enabled us to assign the weight percent of PANI in each synthesized sample. In the DSC results, the degradation of composites taking place at higher temperatures after the incorporation of FA,

indicated that FA has a positive influence on the thermal stability of the composites as its presence delayed their fast degradation.

An investigation of the electrochemical properties showed splitting of the conductance values among the redox states of the composite, which means that the physical properties of the nanorod can be modulated by the application of appropriate electrode potential to make them suitable for specific applications.

From the study of dc conductivity as a function of temperature, it was inferred that both the PANI/FA composites as well as the pure PANI were semiconducting in nature. Moreover, the conductivity was expectedly found to decrease with the addition of FA in PANI. The observed temperature behaviour of conductivity of PANI as well as that of PANI/FA composites was explained on the basis of quasi one-dimensional variable range hopping model. Thus it was concluded that the conductivity in PANI/FA composites is due to the quasi one-dimensional hopping, and therefore, the decrease of conductivity with the addition of FA may be attributed to the localization of charge carriers.

REFERENCES

[1] Shafiq, N; Nuruddin, MF; & Kamaruddin, I; In: *Cement and Concrete Science Conference No. 26*, 2006, Sheffield Hallam University, UK. *Adv. Appl.Ceram.* 2007, **106** (6), 314-318.

[2] Somerset, Vernon Sydwill; The preparation and characterization of high capacity ion exchange adsorbants made by co-disposal of fly ash and acid mine drainage, and their use in electrochemical systems for water purification, 2003, Master's Thesis, Department of Chemistry, University of Western Cape, South Africa.

[3] Hernández, Paola Andrea Benavides; & Esteban, Efren Mendoza; *Sintesis de Zeolitas a partir de cenizas de carbon provenientes de la combustion de la termoelectrica de Zipaquira* (in Spanish), 2007, Chemical Engineering Thesis, School of Chemical Engineering, Industrial University of Santander, Bucaramanga, Colombia.

[4] Yamada, Katsutoshi; Haraguchi, Kensaku; Gacho, Carmel; Wongshiri Bussakorn; & Pena Mary; Paper #116, In: *International Ash Utilization Symposium*, 2003, Centre for Applied Energy Research, University of Kentucky, USA. http://www.flyash.info

[5] Ilic, Marina; Cheeseman, Christopher; Sollars, Christopher; Knight, Jonathan; *Fuel* 2003, **82**, 331-336.

[6] http://www.ashkem.com/product.html

[7] Ayoko, Godwin A; Lim, McKenzie CH; Olofinjana, Ayodele; & Gilbert, Dale; *J. Chem. Technol. Biotechnol.* 2005, **80**, 259-267.

[8] ASTM C618-92a. American Society for Testing and Materials, 1994, *Annual Book of ASTM Standards*, 04.02, West Conshohocken, Pennsylvania.

[9] http://www.flyash.com/flyashenvironment.asp

[10] Iyer, RS; & Scott, JA; *Resour. Conserv. Recycl.* 2001, **31** (3), 217-228.

[11] Petrik, Leslie F; White, Richard A; Klink, Michael J; Somerset, Vernon S; Burgers, Colleen L; & Fey, Martin V; Paper #61, In: *International Ash Utilization Symposium*, 2003, Centre for Applied Energy Research, University of Kentucky, USA. http://www.flyash.info

[12] Rungsuk, Doungmanee; Apiratikul, Ronbanjob; Pavarajarn, Varong; & Pavasant, Prasert; In: *The 2nd Joint International Conference on Sustainable Energy and Environment (SEE 2006)*, 2006, Bangkok, Thailand.
[13] Lin, Cheng-Fang; & His, Hsing-Cheng; *Environ. Sci. Technol.* 1995, **29**, 1109-1117.
[14] Moreno, Natàlia; Querol, Xavier; Ayora, Carlos; Pereira, Constantino Fernández; & Janssen-Jurkovicová, Maria; *Environ. Sci. Technol.* 2001, **35**, 3526-3534.
[15] Hendricks, Nicolette Rebecca; The application of high capacity ion exchange adsorbant material, synthesized from fly ash and acid mine drainage, for the removal of heavy and trace metal from secondary co-disposal process waters; 2005, Master's Thesis, Department of Chemistry, University of Western Cape, South Africa.
[16] Somerset, VS; Petrik, LF; White, RA; Klink, MJ; Key, D; & Iwuoha, E; *Talanta* 2004, **64**, 109-114.
[17] Somerset, Vernon; Petrik, Leslie; & Iwuoha, Emmanuel; *J. Environ. Sci. Health* 2005, **40**, 1627-1636.
[18] Somerset, Vernon; Petrik, Leslie; & Iwuoha, Emmanuel; *J. Environ. Manage.* 2008, **87**, 125-131.
[19] Somerset, Vernon; Petrik, Leslie; Klink, Michael; Etchebers, Olivier; White, Richard; Key, David; & Iwuoha, Emmanuel; *Fresenius Environ. Bull.* 2005, **14** (11), 1-3.
[20] Somerset, Vernon S; Petrik, Leslie F; White, Richard A; Klink, Michael J; Key, David; & Iwuoha, Emmanuel I; *Fuel* 2005, **84**, 2324-2329.
[21] Gitari, WM; Petrik, LF; Etchebers, O; Key, DL; Iwuoha, E; & Okujeni C; *Fuel* 2008, **87**, 1637-1650.
[22] Gitari, WM; Petrik, LF; Etchebers, O; Key, DL; & Okujeni C; *Fuel* 2008, **87**, 2450-2462.
[23] Nollet, Hendrik; Roels, Murielle; Lutgen, Pierre; Van der Meeren, Paul; & Verstraete, Willy; *Chemosphere* 2003, **53** (6), 655-665.
[24] Mozaffari, Morteza; Russelle, Michael P.; Rosen, Carl J.; & Nater, Edward A.; *Soil Sci. Soc. Am. J.* 2002, **66**, 171-178.
[25] Stevens, Gene; & Dunn, David; *J. Environ. Qual.* 2004, **33**, 343-348.
[26] Pathan, SM; Aylmore, LAG; & Colmer, TD; *J. Environ. Qual.* 2003, **32**, 687-693.
[27] Bhattacharya, SS; & Chattopadhyay, GN; *J. Environ. Qual.* 2002, **31**, 2116-2119.
[28] Chandra, Avinash (2008). ASH Resistivity Laboratory at IIT Delhi to Support ESP Performance Improvement in India. http://www.iitd.ernet.in/center/ces/ash.html
[29] Chaudhuri, SP; Sarkar, P; & Chakraborty, AK; *Ceram. Int.* 1999, **25** (1), 91-99.
[30] Karakişla, M; Saçak, M; Erdem E; & Akbulut U; *J. Appl. Electrochem.* 1997, **27**, 309-316.
[31] Raghunathan, Anasuya; Kahol, PK.; Ho, JC; Chen, YY; Yao, YD; Lin, YS; & Wessling, B; *Phys. Rev.* B 1998, **58**, R15955-R15958.
[32] Raghavendra, SC; Khasim, Syed; Revanasiddappa, M; Prasad, MVN. Ambika; & Kulkarni, A.B; *Bull. Mater. Sci.* 2003, **26**, 733-739.
[33] Lee, D; Char, K; Lee, SW; & Park, YW; *J. Mater. Chem.* 2003, **13**, 2942-2947.
[34] Schnitzler, DC; & Zarbin, AJG; *J. Braz. Chem. Soc.* 2004, **15**, 378-384.
[35] Roy, Bidhan C; Dutta Gupta, Maya; Bhowmik, Leena; & Ray, Jayanta K; *Bull. Mater. Sci.* 2001, **24**, 389-396.
[36] Roy, Bidhan C; Dutta Gupta, Maya; Bhowmik, Leena; & Ray, Jayanta K; *Bull. Mater. Sci.* 2003, **26**, 633-637.

[37] Raghavendra, SC; Raibagkar, RL; & Kulkarni, AB; *Bull. Mater. Sci.* 2002, **25**, 37-39.
[38] Narayan, Himanshu; Alemu, Hailemichael; & Iwuoha Emmanuel; *Phys. Stat. Sol.* (a) 2006, **203** (15), 3665-3672
[39] Iwuoha, Emmanuel I; Mavundla, Sipho E; Somerset, Vernon S; Petrik, Leslie F; Klink, Michael J; Sekota, Mantoa; & Bakers, Priscilla; *Microchim. Acta* 2006, **155** (3-4), 453-458.
[40] Cho, MS; Park, SY; Hwang, JY; & Choi, HJ; *Mat. Sci. Eng.* 2004, **24**, 15-18.
[41] Pouget, JP; Jdzefowiczt, ME; Epstein, AJ; Tang, X; & MacDiarmid, AG; *Macromolecules* 1991, **24**, 779-789.
[42] Wolter, A; Rannou, P; Travers, JP; Gilles, B; & Djurado, D; *Phys. Rev.* B 1998, **58**, 7637-7647.
[43] Sperber, Henry; 1995, In: *Insulation material and method using fly ash*, US Patent 5393794. http://www.patentstorm.us/patents/5393794/fulltext.html
[44] Chandrakanthi, RLN; & Careem, MA; *Thin Solid Films* 2002, **417** (1-2), 51-56.
[45] Albuquerque, JE; Mattoso, LHC; Balogh, DT; Faria, RM; Masters, JG; & MacDiarmid, AG; *Synth. Met.* 2000, **113**, 19-22.
[46] Schnitzler, DC; Meruvia, MS.; Hummelgen, IA.; & Zarbin, AJG.; *Chem. Mat.* 2003, **15** (24), 4658-4665.
[47] Pruneanu, S; Veress, E; Marian, I; & Onuciu, L; *J. Mat. Sci.* 1999, **34**, 2733-2739.
[48] Sivakumar, C; Vasudevan, T; Gopalan, A; & Wen, Ten-Chin; *Ind. Eng. Chem. Res.* 2001 **40** (1), 40-51.
[49] Nalwa, SH; ed.; In: *Handbook of Organic Conductive Molecules and Polymers*; John Wiley and Sons: New York, USA, 1997; Vol. 2, 506-537.
[50] Harada, I; Furukawa, Y; & Ueda, F; *Synth. Met.* 1989, **29** (1), 303-312
[51] Cao, Y; *Synth. Met.* 1990, **35** (3), 319-332.
[52] Cao, Y; Smith, P; & Heeger, AJ; *Synth. Met.* 1989, **32** (3), 263-281.
[53] Arenillas, A; Smith, KM; Drage, TC; & Snape, CE; *Fuel* 2005, **84**, 2204-2210.
[54] Pielichowski, Krzysztof; *Solid State Ionics* 1997, **104**, 123-132.
[55] Matveeva, ES; Calleja, R. Diaz; & Parkhutik, VP; *Synth. Met.* 1995, **72** (2), 105-110.
[56] Han, Moon Gyu; Lee, Yong Jin; Byun, Sung Woen; & Im, Seung Soon; *Synth. Met.* 2001, **124** (2-3), 337-343.
[57] Ansari, R; Price, WE; & Wallace, GG; *Polymer* 1996, **37** (6), 917-923.
[58] Cardoso, MJ; Lima, MF; & Lenz, DM; *Materials research* 2007, **10** (4), 425-429.
[59] Basavaraja, R; Pierson, R; Kim, JH; & Huh, DS; *Bull. Korean Chem. Soc.* 2008, **29** (9), 1699-1704.
[60] Perkmez, Nuran; Pekmez, Kadir; & Yildiz, Attila; *J. Electroanal. Chem.* 1994, **370** (1-2), 223-229.
[61] Iwuoha, Emmanuel I; de Villaverde, David Saenz; Garcia, Nuria P; Smyth, Malcolm R; & Pingarron, Jose M; *Biosens. Bioelectronics* 1997, **12** (8), 749-761.
[62] Lu, Xuehong; Xu, Jianwei; & Wong, Limin; *Synth. Met.* 2006, **156** (2-4), 117-123.
[63] Long, Yunze; Chen, Zhaojia; Duvail, Jean Luc; Zhang, Zhiming; & Wan, Meixiang; *Physica* B 2005, **370** (1-4), 121-130.
[64] Stejskal, J; & Gilbert, RG; *Pure Appl. Chem.* 2002, **74**, 857-867.
[65] Wang, ZH; Scherr, EM; MacDiarmid, AG; & Epstein, AJ; *Phys. Rev.* B 1992, **45**, 4190-4202.

[66] Zuo, Fulin; Angelopoulos, Marie; MacDiarmid, Alan G; & Epstein, Arthur J; *Phys. Rev.* B 1987, **36**, 3475-3478.
[67] Kaiser, AB; *Rep. Prog. Phys.* 2001, **64**, 1-49.